JOURNAL OF VIROLOGY, Aug. 2005, p. 10776–10787 Vol. 79, No. 16
0022-538X/05/$08.00+0 doi:10.1128/JVI.79.16.10776–10787.2005

Caveola-Dependent Endocytic Entry of Amphotropic Murine Leukemia Virus

Christiane Beer,[1,2] Ditte S. Andersen,[1]† Aleksandra Rojek,[3] and Lene Pedersen[1,2]*

Department of Molecular Biology,[1] Institute of Clinical Medicine,[2] and Institute of Anatomy,[3] Aarhus University, 8000 Aarhus C, Denmark

Received 7 November 2004/Accepted 24 May 2005

Early results suggested that the amphotropic murine leukemia virus (A-MLV) does not enter cells via endocytosis through clathrin-coated pits and this gammaretrovirus has therefore been anticipated to fuse directly with the plasma membrane. However, here we present data implicating a caveola-mediated endocytic entry route for A-MLV via its receptor Pit2. Caveolae belong to the cholesterol-rich microdomains characterized by resistance to nonionic detergents such as Triton X-100. Extraction of murine fibroblastic NIH 3T3 cells in cold Triton X-100 showed the presence of the A-MLV receptor Pit2 in detergent-insoluble microdomains. Using coimmunoprecipitation of cell extracts, we were able to demonstrate direct association of Pit2 with caveolin-1, the structural protein of caveolae. Other investigations revealed that A-MLV infection in contrast to vesicular stomatitis virus infection is a slow process ($t_{1/2} \approx 5$ h), which is dependent on plasma membrane cholesterol but independent of NH_4Cl treatment of cells; NH_4Cl impairs entry via clathrin-coated pits. Furthermore, expression of dominant-negative caveolin-1 decreased the susceptibility to infection via Pit2 by approximately 70%. These results show that A-MLV can enter cells via a caveola-dependent entry route. Moreover, increase in A-MLV infection by treatment with okadaic acid as well as entry of fusion-defective fluorescent A-MLV virions in NIH 3T3 cells further confirmed our findings and show that A-MLV can enter mouse fibroblasts via an endocytic entry route involving caveolae. Finally, we also found colocalization of fusion-defective fluorescent A-MLV virions with caveolin-1 in NIH 3T3 cells. This is the first time substantial evidence has been presented implicating the existence of a caveola-dependent endocytic entry pathway for a retrovirus.

Amphotropic murine leukemia virus (A-MLV) pseudotypes are widely used in gene therapy trials, and A-MLV and other gammaretroviral envelope proteins are often manipulated, aiming at targeted retroviral gene delivery at the receptor level (48). The basis for efficient and controlled gene delivery is knowledge about the viral entry mechanisms.

Viral entry is initiated by the specific interactions between the viral envelope protein and a cellular receptor. The type III sodium-dependent phosphate transporter Pit2, a multimembrane-spanning protein, was identified as a receptor for A-MLV in 1994; moreover, it is a receptor for the A-MLV-related isolate 10A1 MLV (17, 31, 32, 37, 59, 60). Little is known about the entry mechanism of viruses employing Pit2 for entry, and the current results are seemingly conflicting.

In principle, two general entry pathways exist for enveloped viruses—entry via direct fusion with the plasma membrane and entry via endocytosis. Until recently, the only known endocytic viral entry pathway was endocytosis via clathrin-coated pits. Sensitivity to, e.g., NH_4Cl has been used to discriminate between the two viral entry routes; NH_4Cl inhibits the pinching off of clathrin-coated pits and the acidification of endosomes, thereby impairing viral infection, while direct fusion at the plasma membrane is NH_4Cl insensitive (27, 49). Entry via endocytosis of clathrin-coated pits and entry via direct fusion at the plasma membrane are also referred to as pH-dependent and pH-independent infection, respectively.

In 1990, McClure and coworkers found that A-MLV infection in NIH 3T3 cells and other cell lines is unaffected by NH_4Cl treatment, which led, at that time, to the conclusion that A-MLV enters cells through direct fusion with the plasma membrane (25). Moreover, the authors found that ecotropic murine leukemia virus (E-MLV) infection in NIH 3T3 cells was inhibited by NH_4Cl treatment (25). Katen and coworkers reexamined entry of E-MLV and A-MLV (16) and found that they infect NIH 3T3 cells via the same infection mechanism. They suggested that both viruses enter the cells via an endocytic pathway that does not necessarily include acidic compartments during the infection process (16).

The features of the A-MLV entry pathway described by Katen et al. (16) are in agreement with a caveola-dependent endocytic entry pathway. Caveola-dependent endocytosis was originally identified as entry pathway for simian virus 40 (SV40) (1, 41). Since then, other viruses have been shown to be able to employ caveolae for entry, e.g., echovirus 1 (24) and, very recently, human polyomavirus BK (9) and human coronavirus 229E (36).

Investigations of caveola-dependent entry of SV40 have revealed the characteristics of this new viral entry pathway. It has been described as pH independent, phosphatase dependent,

* Corresponding author. Mailing address: Department of Molecular Biology, Aarhus University, C. F. Møllers Allé, Bldg. 130, DK-8000 Aarhus C, Denmark. Phone: 45-8942-2633. Fax: 45-8619-6500. E-mail: LP@mb.au.dk.

† Present address: Growth Regulation Laboratory, Cancer Research UK London Research Institute, London WC2A 3PX, United Kingdom.

and dependent on plasma membrane cholesterol, and it can be inhibited by expression of dominant-negative caveolin-1 (1, 41).

Caveolae, which are flask-shaped invaginations of the plasma membrane, belong, together with rafts, to the cholesterol-rich microdomains. In these plasma membrane regions, cholesterol molecules are intercalated between the lipid acyl chains and this causes a decrease of fluidity and resistance to nonionic detergents. Caveolae have the same lipid composition as other cholesterol-rich microdomains but consist, in addition, of an important structural protein, caveolin-1 (47). Within the last 10 years, several proteins which are specifically associated with caveolae have been identified (reviewed in references 2 and 52). This association is not only a result of the specific lipid environment of caveolae; proteins containing a caveolin-binding motif can bind directly to caveolin-1 (7).

We show here that the A-MLV and 10A1 MLV receptor Pit2 associates with cholesterol-rich microdomains and we show evidence for direct association with caveolin-1. Moreover, we show that infection via Pit2 has typical characteristics of a caveola-mediated entry process, that is, it is a slow process, pH independent, phosphatase dependent, cholesterol dependent, and inhibited by dominant negative caveolin-1. Moreover, we observed an increase in A-MLV infection by okadaic acid treatment as anticipated for endocytosis via caveolae. Furthermore, by using confocal microscopy, we show that fluorescent fusion-defective A-MLV particles were able to enter NIH 3T3 cells and we also found colocalization of fusion-defective fluorescent A-MLV virions with caveolin-1. Taken together, our data show that entry via Pit2 can occur in a caveola-mediated endocytic manner.

MATERIALS AND METHODS

Cells. NIH 3T3 (ATCC CRL-1658) cells were propagated in Dulbecco's modified Eagle's medium (DMEM) (Gibco BRL) supplemented with 10% newborn calf serum (NCS) (Gibco BRL), 100 IU/ml of penicillin, and 100 μg/ml of streptomycin (Gibco BRL) (DMEM/NCS/PS). 293T cells (ATCC CRL-11268) were propagated in DMEM supplemented with 10% fetal calf serum, 100 IU/ml of penicillin, and 100 μg/ml of streptomycin (DMEM/FCS/PS). CHO K1 (ATCC CRL-61) cells were propagated in α-modified minimal essential medium (α-MEM) (Gibco BRL) supplemented with 10% fetal calf serum, 100 IU/ml of penicillin, and 100 μg/ml of streptomycin (α-MEM/FCS/PS). *Mus dunni* tail fibroblastic (MDTF) cells (a kind gift from Melvyn Yap) were propagated in DMEM/FCS/PS. NIH 3T3 cells overexpressing human Pit2 (K. Madsen, M. M. Kjærgaard, K. Dreyer, P. M. Martensen, and L. Pedersen, unpublished data) were propagated in DMEM/NCS/PS. All cells were grown at 37°C, 10% CO_2 and 95% humidity.

Antibodies. Mouse anti-caveolin-1 antibodies were obtained from BD Bioscience and Transduction Laboratories. Rabbit anti-Pit2 antibodies were generous gifts from David Kabat and Robert B. Gunn (56). For Western blot analyses, pig anti-rabbit immunoglobulin G (DAKOCytomation) or goat anti-mouse immunoglobulin G (Jackson ImmunoResearch), both coupled to horseradish peroxidase, were used as secondary antibodies. For confocal microscopy, an anti-mouse Texas Red-labeled secondary antibody (Molecular Probes) was used as the secondary antibody.

Virus production. A-MLV (4070A isolate) pseudotypes carrying the β-galactosidase-encoding vector G1BgSvN (26) were obtained from the producer cell line PA317GBN (28, 30) (kind gift from M. Eiden). 10A1 MLV pseudotypes carrying G1BgSvN were obtained from the producer cell line PT67GBN (6, 29). PA317GBN and PT67GBN cells were grown in DMEM/NCS/PS. Filtered (0.45-μm pore size) vector supernatants were stored at −80°C. To generate particles carrying the vesicular stomatitis virus (VSV) glycoprotein, plasmids encoding the VSV glycoprotein (Clontech), the Moloney MLV *gag-pol* gene (pHIT60) (53), and a retroviral vector encoding the β-galactosidase gene (pHIT111) (53) were cotransfected into 293T cells; 48 h after transfection, VSV vector pseudotype-containing supernatants were harvested, filtered (0.45-μm pore size), and stored at −80°C until use.

Virus titer. The titers of A-MLV and 10A1 MLV pseudotypes were determined on D17 cells as previously described (39); titers of VSV pseudotypes were determined in a similar set-up on NIH 3T3 cells. The titers obtained were ca. 10^5 blue-forming units/ml for A-MLV and 10A1 MLV and 8×10^5 for VSV; however, in general, diluted stocks were employed.

β-Galactosidase staining of infected cells. The cells were fixed with 0.05% glutaraldehyde (5 min at room temperature) and washed twice with phosphate-buffered saline before they were overlaid with staining solution (5 mM potassium ferricyanide, 5 mM potassium ferrocyanide, 2 mM $MgCl_2$) containing 1 mg/ml X-Gal (5-bromo-4-chloro-3-indolyl-β-D-galactopyranoside). β-Galactosidase-positive (blue) cells were counted under a light microscope.

MBCD treatment. Extraction of cholesterol was performed as described by Lu et al. (23). NIH 3T3 cells were washed once with DMEM without serum and overlaid with DMEM without serum and containing 0 mM (mock treatment), 5 mM, or 10 mM methyl-beta-cyclodextrin (MBCD) (Merck). After incubation at 37°C for 15 min, the cells were washed twice with DMEM without serum.

Infection of MBCD-treated cells. One day prior to MBCD treatment and infection, NIH 3T3 cells were seeded in 24-well plates. The cells were treated with 0 mM, 5 mM, and 10 mM MBCD as described above. After MBCD treatment, cells were infected with serial dilutions of A-MLV (PA317GBN produced, 0.45 μm filtered, 4 μg/ml Polybrene) or VSV (293T produced, 0.45 μm filtered, 8 μg/ml Polybrene) (2 h infection). To inactivate adsorbed but noninternalized viruses, the cells were washed once with citrate buffer (40 mM sodium citrate, 10 mM KCl, 135 mM NaCl, pH 3.1) for 1 min at room temperature (19); they were thereafter grown for 2 days in DMEM–5% NCS and stained for β-galactosidase activity.

Cell cycle analysis. To study the effect of the MBCD treatment on the cell cycle, NIH 3T3 cells were seeded in six-well plates and treated with 0 mM, 5 mM, or 10 mM MBCD as described above, washed once with DMEM without serum, and cultivated with DMEM–5% NCS. After 0, 2, 8, 12, 24, and 48 h of treatment, the cells were brought in suspension with trypsin (Gibco BRL) and pelleted. They were fixed by dropwise addition of −20°C 70% ethanol while vortexing and stored at −20°C until further investigation. The fixed cells were prepared for analyses of DNA content by pelleting and subsequent resuspension in phosphate-buffered saline containing 20 μg/ml RNase A (Sigma). Finally, they were passed through 35-μm filters (Falcon) and incubated with 100 μg/ml propidium iodide. The DNA content of the cells was analyzed by flow cytometry (FACS-Calibur, BD) and the resulting histograms were analyzed using the Dean-Jett-Fox model of the FlowJo 4.4.3 software.

Cholesterol staining. NIH 3T3 cells were seeded on chamber slides (Nunc) and grown to 50% confluence. For cholesterol staining after MBCD treatment, the cells were overlaid with filipin (50 μg/ml in phosphate-buffered saline, Sigma) and incubated for 1 h at room temperature. A fluorescence microscope (IX70, Olympus; filter sets: filipin XF113, 387/450 nm [Em/Ex], Omega filters) with a 1,000x magnification was used for the detection of stained cells. Images were taken with a Colorview II camera (Olympus). Brightness and contrast were adjusted (Adobe Photoshop).

NH_4Cl treatment. One day prior to NH_4Cl treatment and infection, NIH 3T3 cells were seeded in 24-well plates. The cells were treated with 50 mM NH_4Cl for 30 min, washed, and infected with A-MLV (PA317GBN derived, 0.45 μm filtered). After 5, 15, 30, and 60 min, noninternalized viruses were inactivated using citrate buffer. Forty-eight hours after infection, the cells were stained for β-galactosidase activity.

Triton X-100 extraction. T75 flasks with cells were washed once with phosphate-buffered saline, overlaid with 1 ml 4°C 0.5% Triton X-100 in the presence of the protease inhibitor Pefabloc (Merck), and gently shaken on ice for 1 min. The supernatant containing the Triton X-100-soluble proteins was removed and stored on ice. The remaining cell remnants (insoluble fraction) were suspended in 1 ml lysis buffer (300 mM NaCl, 50 mM Tris-HCl, 1% Triton X-100, 2 mM Pefabloc) and homogenized by intensive pipetting. Equal volumes of soluble and insoluble fractions were used for Western blot analysis.

Coimmunoprecipitation. T75 flasks with cells were suspended in lysis buffer (300 mM NaCl, 50 mM Tris-HCl, 1% Triton X-100, 2 mM Pefabloc) at room temperature and homogenized by intensive pipetting. The samples were incubated with anti-Pit2 (from David Kabat) or 5 μg anti-caveolin-1 associated protein A beads (Dynal). Using the magnetic separation system from Dynal, the samples were washed and the bound proteins were removed with citrate buffer (pH 3.0) as described by the manufacturer before use for sodium dodecyl sulfate (SDS)-polyacrylamide gel electrophoresis (PAGE) and Western blot analyses.

SDS-PAGE and Western blotting. Samples were mixed with gel loading buffer (125 mM Tris, 5% SDS, 12.5% β-mercaptoethanol, 50% glycerol, 0.25% brom-

phenol blue) and loaded on an SDS-PAGE gel using 12% and 3% acrylamide for the resolution and stacking gels, respectively. After separation, the proteins were transferred to an Immobilon-P polyvinylidene difluoride membrane (Millipore). The membrane was blocked for 30 min with Tris-buffered saline containing 0.1% Tween 20. To detect Pit2 or caveolin-1 proteins, the membranes were incubated with antibodies (1:1,000 dilution) against these proteins in blocking buffer. The secondary antibodies, pig anti-rabbit and goat anti-mouse (both coupled to horseradish peroxidase), were used at a 1:2,000 and 1:1,000 dilutions, respectively. The blots were developed in ECL solution.

Transient cotransfections and infection assays. Transient transfection and infection assays were performed essentially as described elsewhere (6, 39). CHO K1 cells were seeded in 60-mm dishes at 2×10^3 cells/cm^2. The next day, the cells were cotransfected by calcium phosphate DNA precipitation. Each precipitate (1 ml) contained 5 μg of pOJ74 (Wyeth-Ayerst Research, Pearl River, NY) encoding human Pit2 (39) or pcDNA3 (empty vector), 2.5 μg of C- or N-terminally green fluorescent protein (GFP)-tagged caveolin-1 expression plasmid in pEGFP-derived vectors from Clontech (kind gifts from Ari Helenius) (41) and 7.5 μg of pUC19 plasmid as a carrier. Aliquots of 200 μl precipitate were used per 60-mm dish, and three independent precipitates (three dishes) were made for each combination. Twenty hours after transfection, media were withdrawn from the dishes, and 2 ml CHO K1-conditioned medium was added to each dish. Four hours later, the cells were infected with 10A1 MLV (1.5 ml PT67GBN supernatant diluted 1:1 with CHO K1-conditioned medium) adjusted to 8 μg/ml of Polybrene; after 4 h, the Polybrene was diluted to a final concentration of 2 μg/ml with CHO K1-conditioned medium. Forty-eight hours after transfection, the cells were fixed and stained for β-galactosidase activity.

The effect of transient expression of the two caveolin-1 constructs on cell growth was analyzed as follows. Precipitates (1 ml) were made which contained 5 μg of the retroviral β-galactosidase encoding vector pLZSN, 2.5 μg of C- or N-terminally GFP-tagged caveolin-1 expression plasmid or 2.5 μg of pEGFP-N1 (empty vector), and 7.5 μg pUC19 plasmid as a carrier. Aliquots of 200 μl precipitate were used per 60-mm dish, and three independent precipitates (three dishes) were made for each combination. Forty-eight hours after transfection, the cells were fixed and stained for β-galactosidase activity.

Okadaic acid treatment. One day prior to okadaic acid treatment and infection, NIH 3T3 cells were seeded in 24-well plates. NIH 3T3 cells were incubated with A-MLV (PA317GBN derived, 0.45 μm filtered) or VSV (293T derived, 0.45 μm filtered) for 4 or 6 h, washed with medium, and subjected to mock treatment (1:100 dimethyl sulfoxide in medium) or 0.1 μM okadaic acid (10 μM stock solution in dimethyl sulfoxide) for 60 min. Subsequently, noninternalized viruses were inactivated by citrate buffer wash and 48 h after infection, the cells were stained for β-galactosidase activity.

Alternatively, NIH 3T3 cells were subjected to mock treatment (1:100 dimethyl sulfoxide in medium) or 0.1 μM okadaic acid for 60 min to remove cell surface caveolae. Subsequently, the cells were infected with A-MLV or VSV for 4 or 6 h in the presence of dimethyl sulfoxide or 0.1 μM okadaic acid. Noninternalized viruses were inactivated using citrate buffer and 48 h after infection, the cells were stained for β-galactosidase activity.

Production of Gag-YFP A-MLV. For production of yellow fluorescent protein (YFP)-tagged fusion-defective A-MLV particles (Gag-YFP A-MLV particles), 293T cells were seeded in T75 flasks and grown to 70% confluence. The cells were transiently cotransfected with a Gag-YFP construct (encoding Moloney MLV Gag structural proteins and a YFP-tagged nucleocapsid protein) (3), pHIT111 (harboring a β-galactosidase-encoding retroviral vector) (53), and a pHIT-derived vector encoding the A-MLV (4070A isolate) envelope. Forty-eight hours after transfection, the supernatants were filtered (0.45 μm) and stored until use at −80°C.

Entry of fusion-defective Gag-YFP A-MLV. For the investigation of the uptake of fusion-defective Gag-YFP A-MLV particles, NIH 3T3 cells were incubated with these viral particles for 6 h at 37°C, washed with phosphate-buffered saline and citrate buffer, and fixed using 4% paraformaldehyde. The plasma membrane of the cells was subsequently stained using rhodamine-labeled concanavalin A (Vector Laboratories, Burliggane, CA). The confocal images were captured with a Leica TCS SP confocal Microscope (Leitz). YFP and rhodamine were excited individually using argon laser 488 nm line and green helium neon laser 543 nm line, respectively. The two single-color images were subsequently merged into a red-green-blue (RGB) image.

Colocalization of fusion-defective Gag-YFP A-MLV with caveolin-1. For investigation of the colocalization of fusion-defective Gag-YFP A-MLV particles with caveolin-1, NIH 3T3 cells were incubated with these viral particles for 6 h at 37°C and washed with phosphate-buffered saline. The cells were permeabilized with 0.25% Triton X-100 and fixed using 4% paraformaldehyde. The cells were subsequently stained for caveolin-1 using mouse anti caveolin-1 antibody (Transduction Laboratories), washed and incubated with an anti-mouse Texas Red labeled secondary antibody (Molecular Probes). Confocal images were captured with a Leica TCS SP confocal Microscope (Leitz). YFP and Texas Red were excited individually using argon laser 488 nm line and green helium neon laser 543 nm line, respectively. The two single-color images were subsequently merged into a RGB image.

Statistical analysis. Receptor functions are presented as mean ± standard deviation. The hypothesis that two mean values were identical was tested by a two-tailed Student's *t* test; values were considered different at a 95% confidence level.

RESULTS

A-MLV infection is a pH independent and slow process. A-MLV infection has been shown to be pH independent (25). In addition, Katen and coworkers have provided data suggesting that A-MLV enters through an endocytic pathway (16). A possible endocytic pathway which is pH independent is caveola-mediated entry (41) and we have here investigated whether caveolae could play a role in entry of A-MLV.

First, we investigated if A-MLV infection is pH independent in our hands using an experimental set-up similar to that of Katen et al. (16). NIH 3T3 murine fibroblasts were treated with 50 mM NH_4Cl, which inhibits entry via clathrin-coated pits (27, 49), before they were exposed to A-MLV (Fig. 1A). After the indicated time periods, noninternalized viruses were inactivated using citrate buffer. As expected and shown by others (16, 25), NH_4Cl treatment did not inhibit A-MLV infection. Mock and NH_4Cl-treated cells were equally susceptible to A-MLV (Fig. 1A) confirming that A-MLV entry is pH independent, that is, independent of clathrin-coated pits. The citrate wash inactivates noninternalized virus but does not influence the viral infection (16; data not shown).

Interestingly, although we infected the cells with a multiplicity of infection of > 1, only approximately 5% of the cells were infected after 1 h of virus exposure (data not shown). To investigate the infection kinetics of A-MLV, we infected NIH 3T3 cells and inactivated noninternalized viruses after different time periods. A-MLV infection of NIH 3T3 cells reached the half-maximal infection level ($t_{1/2}$) about 5 h after virus addition whereas an MLV core pseudotyped with VSV glycoprotein reached $t_{1/2}$ after just 1.5 h (Fig. 1B); VSV enters cell via clathrin-coated pits (8).

To investigate whether A-MLV binding to the cells was a limiting factor, we incubated NIH 3T3 cells for different time periods with a fluorescently labeled A-MLV where the nucleocapsid protein is tagged with YFP (3). As shown in Fig. 1C, cell-bound viral particles could be detected 5 min after addition of the viral supernatant. Mock-treated cells did not show any fluorescent signal (data not shown). Binding of YFP-tagged A-MLV to glass surface and size comparison with 110-nm Texas Red-labeled beads show that the viral particles are separated from each other and do not have the tendency to aggregate (Fig. 1D). These results demonstrate that binding of A-MLV to cells is not the limiting factor and not the reason for the slow infection process.

Entry kinetics alone were also analyzed. Thus, A-MLV and VSV pseudotyped particles were bound to MDTF cells at 4°C, and the cells were washed with medium to remove unbound viruses and incubated at 37°C for the indicated time periods at which noninternalized viruses were inactivated. As expected from the infection kinetics (Fig. 1B), A-MLV needed approx-

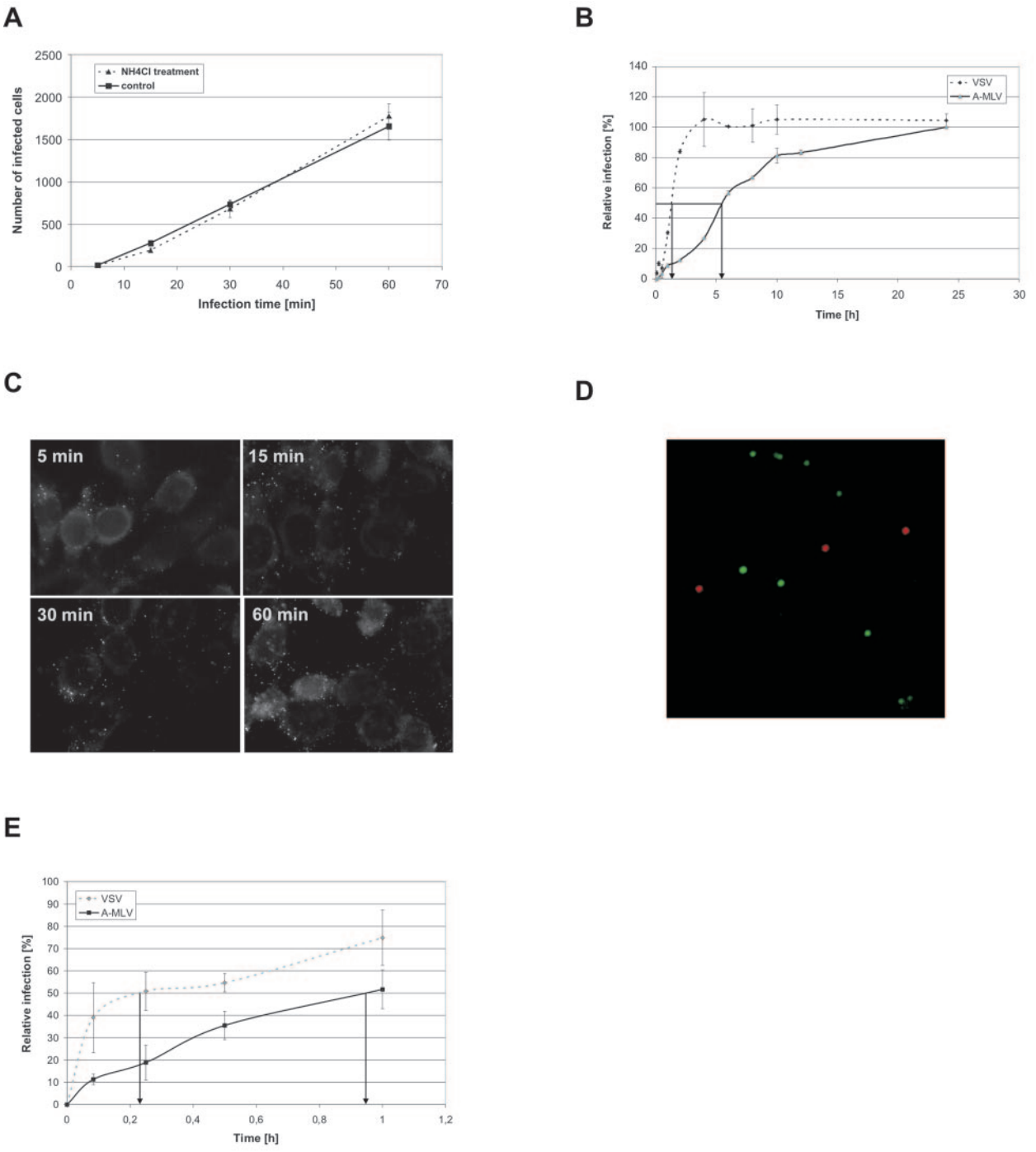

FIG. 1. Infection of NIH 3T3 is a slow pH-independent process. (A) NH_4Cl treatment has no effect on A-MLV infection. NIH 3T3 cells were treated with 50 mM NH_4Cl for 30 min, washed, and incubated with A-MLV pseudotyped vectors. At the indicated time points, noninternalized viruses were inactivated using citrate buffer. Forty-eight hours after vector addition, infected β-galactosidase-positive cells were counted. Shown is one representative experiment done in triplicate. Similar results were obtained in another independent experiment. (B) Infection kinetics of A-MLV and VSV pseudotyped vectors. NIH 3T3 cells were exposed to A-MLV or VSV pseudotyped vectors and at the indicated time points, noninternalized viruses were inactivated using citrate buffer. Forty-eight hours after vector addition, infected β-galactosidase-positive cells were counted. The number of infected cells is normalized to the 24-h value. Shown is one representative experiment done in duplicate. Similar results were obtained in a second independent experiment. (C) Binding kinetics of fluorescently labeled A-MLV. NIH 3T3 cells were incubated with A-MLV particles containing a YFP-labeled nucleocapsid protein. At the indicated time points, cells were washed, fixed, and analyzed by fluorescence microscopy; particles not in focus in the cell cultures can appear larger than a single particle. Pictures were taken with an oil-immersion objective (original magnification, 1,000×). (D) Size comparison of fluorescent A-MLV with 110-nm fluorescent beads. A-MLV and 110-nm Texas Red-labeled beads were bound to chamber slides in the presence of Polybrene. After fixation with paraformaldehyde, pictures were taken with an oil-immersion objective (original magnification, 1,000×). (E) Entry kinetic of A-MLV and VSV. A-MLV or VSV pseudotypes were bound to MDTF cells at 4°C, the cells were washed to remove unbound virus, incubated at 37°C, and at the indicated time points, noninternalized viruses were inactivated using citrate buffer. Forty-eight hours after vector addition, infected β-galactosidase-positive cells were counted. The number of infected cells is normalized to the 24-h value. Values are the average of two independent experiments done in duplicate.

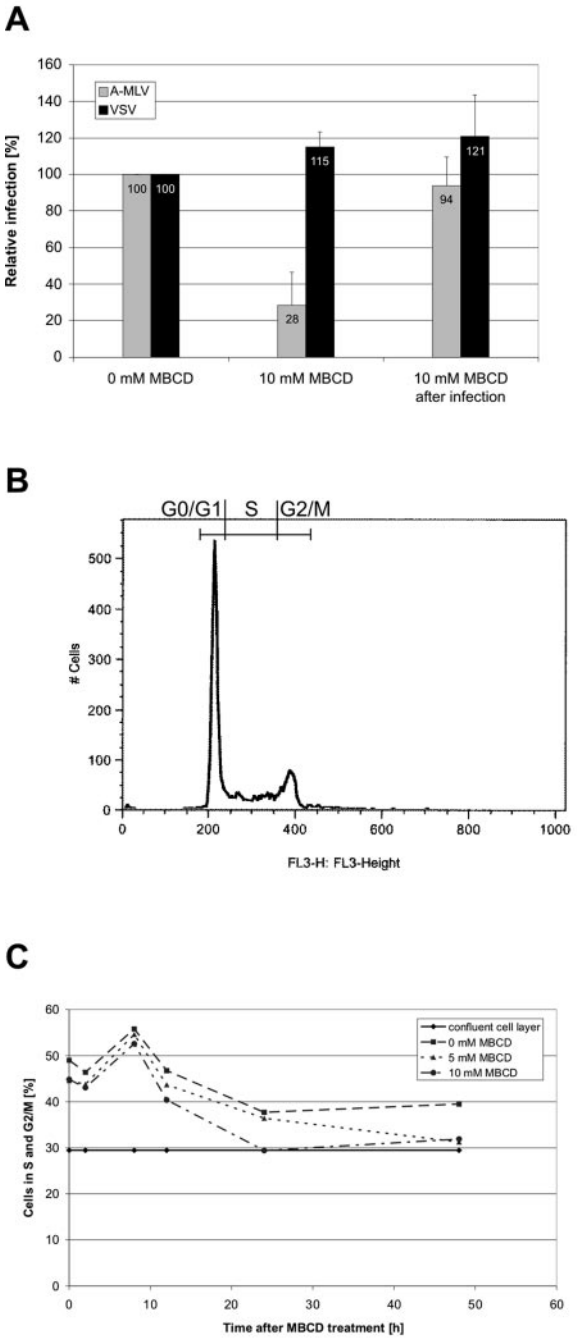

FIG. 2. MBCD treatment of NIH 3T3 cells. (A) MBCD decreases the susceptibility of NIH 3T3 cells to A-MLV infection. NIH 3T3 cells were treated with 10 mM MBCD at 37°C for 15 min and infected for 2 h with A-MLV or VSV pseudotyped vectors. Noninternalized viruses were removed by citrate wash and 2 days after vector addition, infected β-galactosidase-positive cells and noninfected cells were counted and the percentages of infected cells was calculated. As a control, NIH 3T3 cells were infected for 2 h with A-MLV or VSV, washed with citrate buffer, and treated with 10 mM MBCD at 37°C for 15 min. The infection levels shown are normalized to the infection levels in the control cultures. Values are the average of two independent experiments done at least in triple; for A-MLV P values were ≤ 0.001 (MBCD treatment before infection) and >0.5 (MBCD treatment after infection), respectively, compared to mock-treated (0 mM MBCD) cultures. (B and C) Investigation of the effect of MBCD treatment on the cell cycle. NIH 3T3 cells were treated with 0 mM (mock), 5 mM, or 10 mM MBCD at 37°C for 15 min. The cells were washed and fresh DMEM containing 5% NCS was added. At 0, 2, 8, 12, 24, and 48 h after treatment, the cells were harvested and analyzed for their DNA amount using flow cytometry. (B) An example of a typical flow cytometry analysis is shown (0 mM MBCD, 2 h after treatment). (C) Fractions of cells in the S and G_2/M phase of the cell cycle after MBCD treatment. At every time point is shown the fractions of cells in S and G_2/M in mock-treated (0 mM MBCD) cultures and cultures treated with 5 mM and 10 mM MBCD. The straight line depicts the fraction of cells in S and G_2/M in an NIH 3T3 cell culture exhibiting only slightly more cell-cell contacts than the 48 h mock- and MBCD-treated cultures to illustrate the proliferative state of the used NIH 3T3 cells in a nonmanipulated culture.

imately four times longer to enter the cells and to reach $t_{1/2}$ than VSV (Fig. 1E). Slow entry kinetics is one of the characteristics of a caveola-dependent entry.

A-MLV infection is dependent on plasma membrane cholesterol. Caveolae belong to cholesterol-rich microdomains and MBCD is often used to investigate whether an infection is dependent on these microdomains. It is known to extract cholesterol out of the plasma membrane of eukaryotic cells (18) leading to disruption of cholesterol-rich microdomains and release of associated proteins (13).

NIH 3T3 cells were mock-treated or treated with 5 mM or 10 mM MBCD, and thereafter infected with A-MLV for 2 h before noninternalized viral particles were inactivated with citrate buffer. Forty-six hours later, the number of infected cells was counted and the percentages of infected cells were calculated and related to the percentages of infected cells in the mock-treated cultures. As a control, NIH 3T3 cells were infected for 2 h, washed with citrate to inactivate noninternalized viral particles and then treated with 10 mM MBCD to determine whether the MBCD treatment itself had an effect on viral infection after internalization. As shown in Fig. 2A, the susceptibility of MBCD-treated cells to A-MLV was reduced by 72%, whereas MBCD treatment after A-MLV infection had no effect. Treatment with 5 mM MBCD resulted in a reduction in the susceptibility to A-MLV by 39% ± 6% (data not shown). As expected, MBCD treatment had no inhibitory effect on infection with a VSV pseudotype, which is known to enter cells via clathrin-coated pits (8).

To investigate whether the MBCD treatment conditions indeed were sufficient to extract cholesterol out of the plasma membrane, we treated NIH 3T3 cells with 5 mM or 10 mM MBCD for 15 min at 37°C and stained the cells with filipin. This fluorescent polyene macrolide antibiotic binds specifically to cholesterol and is used for the detection of cholesterol in, e.g., plasma membranes (11). Fluorescence microscopy revealed that the MBCD treatment reduced the amount of cholesterol in the plasma membrane (Fig. 3). Determination of the mean fluorescence using photo analyzing software showed that treatment of NIH 3T3 cells with 5 mM MBCD decreased plasma membrane cholesterol by 36% compared to mock-treated cells, while treatment with 10 mM MBCD led to a 73% reduction (Fig. 3E).

Although the main part of the cholesterol was depleted using 10 mM MBCD there was no obvious lethal effect when investigating the cells in a light microscope. However, since A-MLV can successfully infect only dividing cells it is impor-

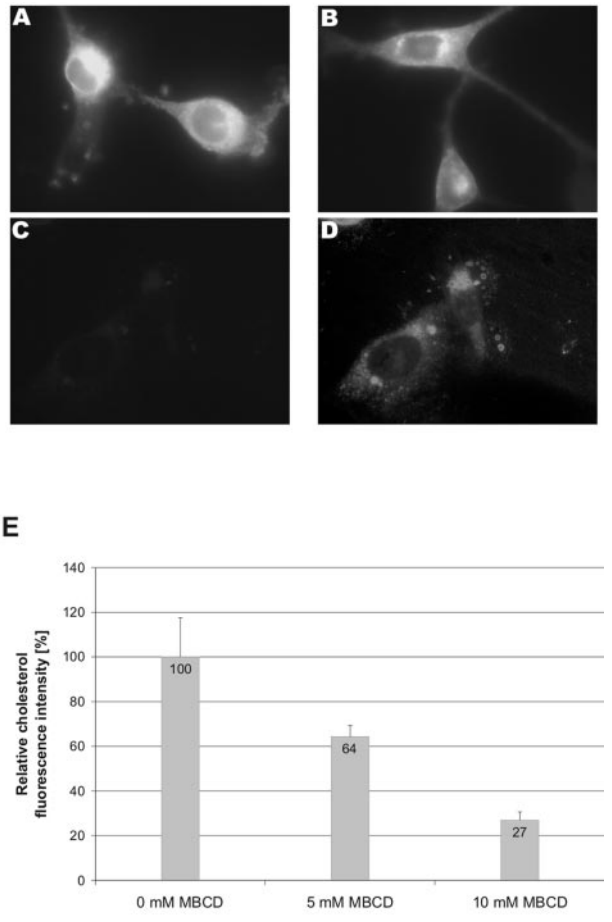

FIG. 3. Effect of MBCD treatment on the plasma membrane cholesterol level of NIH 3T3 cells. NIH 3T3 cells were treated with (A) 0 mM (mock), (B) 5 mM, or (C and D) 10 mM MBCD at 37°C for 15 min. After this treatment, the cells were fixed and stained with 50 μg/ml filipin for 1 h. Pictures were all taken with an oil-immersion objective (original magnification, 1,000×) using the same camera settings. (A to C) Unprocessed pictures; (D) copy of the picture in C, which has been processed in Adobe Photoshop to visualize the presence of the cells. (E) Quantification of cholesterol extraction. Pictures of mock (0 mM) and MBCD-treated NIH 3T3 cells were analyzed for their fluorescently labeled cholesterol. The cholesterol levels shown are normalized to that of mock-treated cells. At least six randomly taken pictures were measured.

tant to know how the MBCD treatment influences the cell cycle. Therefore, we treated NIH 3T3 cells with 5 mM or 10 mM MBCD for 15 min at 37°C, harvested the cells 0, 2, 8, 12, 24, and 48 h after treatment, stained for DNA with propidium iodide, and analyzed for the amount of DNA using flow cytometry. The DNA amount and the resulting fluorescence reflect the stage of the cell cycle. A typical curve for DNA fluorescence measurement via flow cytometry is shown in Fig. 2B. The percentage of cells arrested in the different stages of the cell cycle was determined using the FlowJo cell cycle analyzing software. Twelve hours after MBCD treatment, the cholesterol depletion caused a decrease in the fraction of dividing cells (S and G_2/M phase) of 3% (5 mM) and 6% (10 mM), respectively, compared to mock-treated cells (Fig. 2C); the maximal decrease of 8% (5 mM MBCD) and 8% (10 mM MBCD) was reached 48 h after treatment compared to mock-treated cells.

These data demonstrate that the reduced A-MLV infection level was not due to an impaired cell cycle, and thus A-MLV infection is dependent on plasma membrane cholesterol.

Pit2 is directly associated with caveolin-1. The slow, pH-independent but cholesterol-dependent infection route supports an involvement of caveolae in A-MLV entry. We therefore investigated whether the A-MLV receptor Pit2 is associated with caveolae. First, we analyzed whether Pit2 in general associates with cholesterol-rich microdomains. It has been shown that proteins localized within these microdomains are insoluble in nonionic detergents such as Triton X-100 at 4°C (51). Therefore, we treated NIH 3T3 cells with Triton X-100 at 4°C and isolated the soluble and insoluble protein fractions. These were analyzed by Western blot using an anti-Pit2 antibody (Fig. 4). Pit2 proteins were present in the soluble as well as in the insoluble fractions, and thus at least a part of the Pit2 protein in the cell is associated with cholesterol-rich microdomains. Similar results were obtained using NIH 3T3 cells overexpressing human Pit2 (data not shown).

To investigate whether Pit2 directly associates with caveolin-1 and caveolae, we performed coimmunoprecipitation studies. For this purpose, NIH 3T3 cells overexpressing human Pit2 were lysed in Triton X-100 at room temperature to disperse cholesterol-rich microdomains. The cell lysate was immunoprecipitated with antibodies to caveolin-1 or Pit2 and the resulting precipitates were analyzed for the content of Pit2 or caveolin-1, respectively. As shown in Fig. 4B, the caveolin-1 antibody recognized caveolin-1 in the Pit2 immunoprecipitate. Two strong bands were detected, which correspond to the monomeric (≈24 kDa) and the dimeric forms (≈48 kDa) of caveolin-1. Correspondingly, Pit2 protein could be detected in the caveolin-1 immunoprecipitate (Fig. 4C). These results are in agreement with the findings from the Triton X-100 treatment of cells at 4°C, which showed that a part of Pit2 is associated with cholesterol-rich microdomains.

Immunoprecipitation using anti-caveolin-1 antibody resulted in two bands recognized by the anti-Pit2 antibody (Fig. 4C). To ensure that the anti-Pit2 antibody used in these experiments was specific, we immunoprecipitated Pit2 using the same anti-Pit2 antibody and analyzed the immunoprecipitate using Western blot and another anti-Pit2 antibody. The results confirmed the specificity of the antibody (data not shown).

These results demonstrate that under the cell culture conditions used a fraction of the Pit2 protein is localized in cholesterol-rich microdomains and that at least a fraction of Pit2 is directly associated with caveolin-1.

Overexpression of dominant-negative caveolin-1 decreases infection via Pit2. The direct association of Pit2 with caveolin-1 further supports that caveolae are involved in viral entry via Pit2. To directly address the role of caveolae in Pit2-mediated entry, we used an N-terminally GFP-tagged caveolin-1 (GFP-cav-1), which functions as a dominant-negative caveolin-1. GFP-cav-1 inhibits caveola-mediated entry of SV40 (41), whereas cav-1-GFP, a C-terminally GFP-tagged caveolin-1, behaves like wild-type caveolin-1 (41, 55).

NIH 3T3 cells are susceptible to Pit2's cognate viruses A-MLV and 10A1 MLV, which hinders direct investigation of the effect of dominant-negative caveolin-1 expression on viral in-

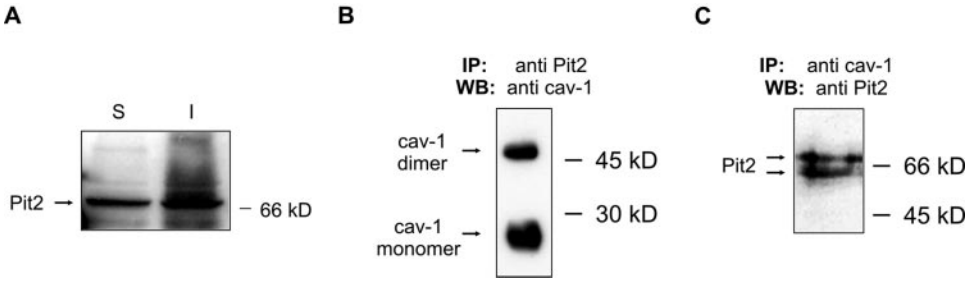

FIG. 4. Pit2 localization and interaction with caveolin-1. (A) Immunoblot analysis of Triton X-100 soluble (S) and insoluble (I) fractions for the presence of Pit2. NIH 3T3 cells were treated with 0.5% Triton X-100 for 1 min at 4°C. The supernatant containing the soluble fraction and the cell remnant-containing insoluble fraction, respectively, were separated by SDS-PAGE and analyzed by immunoblot for the presence of Pit2 proteins. Similar results were obtained using NIH 3T3 cells overexpressing human Pit2 (not shown). (B) Caveolin-1 coimmunoprecipitate with Pit2. NIH 3T3 cells overexpressing human Pit2 were lysed at room temperature in 1% Triton X-100 and lysates were immunoprecipitated with an anti-Pit2 antibody. The resulting immunoprecipitates were analyzed for the presence of caveolin-1 using SDS-PAGE and immunoblotting. (C) Pit2 coimmunoprecipitate with caveolin-1. NIH 3T3 cells overexpressing human Pit2 were lysed at room temperature in 1% Triton X-100 and lysates were immunoprecipitated with an anti-caveolin-1 antibody. The resulting immunoprecipitates were analyzed for the presence of Pit2 using SDS-PAGE and immunoblotting. IP, immunoprecitation; WB, Western blot (immunoblotting). The anti-Pit2 antibodies recognize both human and mice Pit2. When using an antibody to a multimembrane-spanning protein not harboring a caveolin-binding consensus sequence, no caveolin-1 was coimmunoprecipitated nor could the protein be detected in lysates immunoprecipitated with anti-caveolin-1 antibodies (not shown).

fection in these cells. However in another study, we found that expression of GFP-cav-1 decreases infection of NIH 3T3 cells expressing a Pit2 mutant, which supports infection with feline leukemia virus B (D. S. Andersen, C. Beer, and L. Pedersen, manuscript in preparation). We here used CHO K1 cells in a transient transfection assay to directly study the effect of caveolin-1 expression on infection via wild-type Pit2. CHO K1 cells were cotransfected with human Pit2 (pOJ74) and an empty vector, cav-1-GFP, or GFP-cav-1. Twenty-four hours after transfection, the cells were infected with 10A1 MLV derived from the PT67 packaging cell line.

Expression of dominant-negative GFP-cav-1 decreased the viral infection level by approximately 70% compared to cells expressing human Pit2 together with an empty vector (Fig. 5). Expression of cav-1-GFP, which behaves like wild-type caveolin-1, had only a negligible effect on the infection, suggesting that the down-regulatory effect was not due to a general inhibitory effect on cell proliferation caused by overexpressed caveolin-1. In addition, the effect of transient expression of GFP-cav-1 and cav-1-GFP on cell proliferation was evaluated but no significant difference in the number of cell divisions were observed between cells transfected with GFP-cav-1 or cav-1-GFP expression plasmids and cells transfected with empty vector (data not shown). These observations make it highly unlikely, although they not entirely rule out, that the observed effect is caused by a general effect of GFP-cav-1 on the cells. Thus, in line with previous studies on SV40 entry (41), we interpret the observed effect of dominant-negative caveolin-1 on viral infection via Pit2 as a result of impaired caveolar function. These data strongly implicate a role of caveolae in gammaretroviral entry via Pit2.

Okadaic acid treatment affects A-MLV infection. Viral entry via caveolae is dependent on phosphatases (42). Okadaic acid is an inhibitor of phosphatases 1 and 2A, and treatment with okadaic acid has been shown to induce endocytosis and thus removal of caveolar structures from the cell surface (38). Moreover, okadaic acid was shown to inhibit endocytosis via clathrin-coated pits (38). Thus, pretreatment of cells with okadaic acid impairs entry via both endocytic pathways, and we therefore investigated whether it impaired A-MLV and VSV entry. In one set of experiments, NIH 3T3 cells were treated with okadaic acid before the cells were exposed to A-MLV or VSV vector pseudotypes in the presence of okadaic acid and noninternalized viruses were inactivated 4 or 6 h after vector exposure. As expected, this experimental setting resulted in a decrease in A-MLV as well as in VSV infection (Fig. 6A). Compared to 4 h, 6 h okadaic acid exposure had a more pronounced effect on the viral infection (Fig. 6A). Okadaic acid can be washed out (38), and it is possible that more vectors captured in the process of endocytosis are capable of

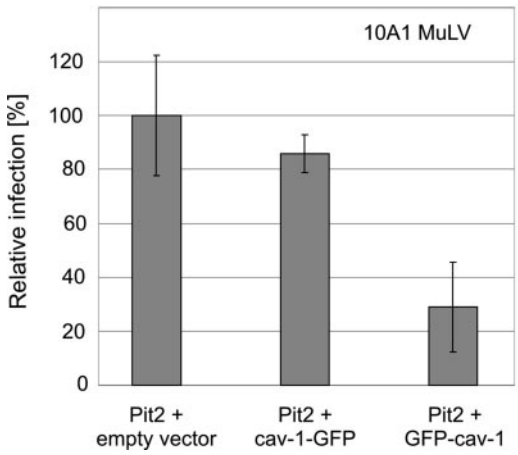

FIG. 5. Retroviral entry via Pit2 is dependent on caveolin-1. CHO K1 cells were cotransfected with a Pit2 expressing plasmid (POJ74) and an empty vector, or cav-1-GFP or GFP-cav-1 expression plasmids as described in Materials and Methods. The following day, cells were exposed to 10A1 MLV pseudotyped vectors encoding β-galactosidase. The data shown represent the means of the number of blue cells from three independent transfections ± standard deviation ($P = 0.356$ and $P = 0.011$ comparing empty vector with cav-1-GFP and with GFP-cav-1, respectively). The number of blue cells per dish was normalized to the number of blue cells per dish cotransfected with POJ74 and the empty expression vector. No blue cells were detected in mock-transfected (empty vectors) cells (data not shown).

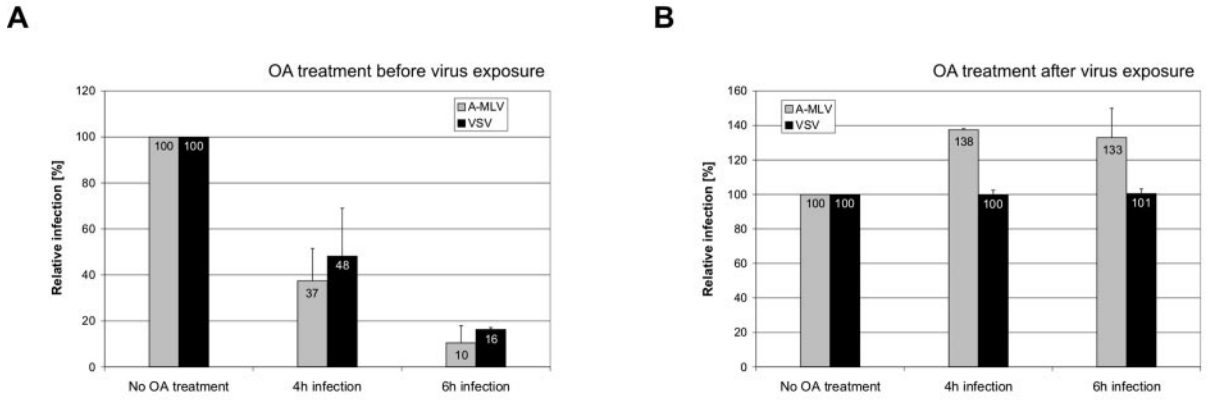

FIG. 6. Effect of okadaic acid on A-MLV and VSV infection. (A) NIH 3T3 cells were treated with 0.1 μM okadaic acid (OA) for 30 min. Subsequently, the cells were infected with A-MLV or VSV pseudotyped vectors for 4 and 6 h in the presence of okadaic acid. Noninternalized viruses were inactivated using citrate buffer and 48 h after vector addition, infected β-galactosidase-positive cells were counted. The numbers of infected cells are normalized to the mock values. Shown are the means of three (A-MLV) or two (VSV) independent experiments done in duplicate. (B) NIH 3T3 cells were incubated with A-MLV or VSV pseudotyped vectors for 4 or 6 h, washed, and treated with 0.1 μM okadaic acid for 30 min. Subsequently, noninternalized viruses were inactivated using citrate buffer and 48 h after vector addition, infected β-galactosidase-positive cells were counted. The numbers of infected cells are normalized to the mock values. Shown are the means of two independent experiments done in duplicate.

completing their infection after 4 h of blocking of the pathways than after 6 h of blocking of the pathways.

In another set of experiments, the cells were treated with okadaic acid after virus exposure. Thus, NIH 3T3 cells were infected with A-MLV or VSV for 4 or 6 h, washed, and treated with okadaic acid; noninternalized viral particles were subsequently inactivated using citrate buffer. Okadaic acid treatment after virus binding enhanced A-MLV entry (Fig. 6B). This observation is in agreement with a stimulation of endocytosis of caveolae (38) and supports a caveola-mediated endocytic entry pathway of A-MLV. As expected from the studies of VSV infection and entry kinetics in Fig. 1B and E, respectively, this treatment had no effect on the VSV infection.

These data further confirm that A-MLV can use caveolae for entry and furthermore implicate endocytosis as entry mechanism.

Fusion-defective A-MLV can enter NIH 3T3 cells and colocalize with caveolin-1. The okadaic acid experiments strongly suggested that A-MLV can infect NIH 3T3 cells using an endocytic entry pathway. An endocytic pathway should allow entry of fusion-defective viral particles. We therefore investigated whether such A-MLV particles can enter NIH 3T3 cells. The particles were made by transiently cotransfecting 293T cells with a retroviral vector, an A-MLV envelope protein-encoding plasmid, and a Gag-YFP construct. In the last construct, the nucleocapsid protein encoded was tagged with YFP (3), which results in the lack of viral enzymes in the viral particle. This leads to unprocessed envelope proteins and therefore to noninfectious and fusion-defective viral particles. Forty-eight hours after transfection, the Gag-YFP A-MLV particles were harvested and tested for their fluorescence and infectivity. As expected, the viral particles exhibited a strong fluorescence but were noninfectious (data not shown).

NIH 3T3 cells were incubated with these particles for 6 h at 37°C and washed with citrate buffer before fixation. Citrate buffer removes viral particles which are not closely associated with the membrane or internalized. The plasma membrane was stained using a rhodamine-labeled lectin and the cells were investigated for the presence of intracellular fusion-defective Gag-YFP A-MLV particles using three-dimensional scanning confocal microscopy. Possibly due to the citrate treatment immediately before fixation, the intracellular membranes were partly stained. Despite this, it was possible to detect intracellular A-MLV particles (Fig. 7A). In each cell investigated, we were able to identify between one and five intracellular viral particles, which were clearly surrounded by the plasma membrane (Fig. 7A and pink arrows in 7B). Furthermore, we detected a number of particles which were not clearly intracellular but seemed to stick within the plasma membrane (Fig. 7B, yellow arrows).

We furthermore investigated whether Gag-YFP A-MLV particles colocalize with caveolin-1. As expected from the data presented, the viral particles colocalize with caveolin-1not only at the cell surface but also intracellularly (Fig. 8). However, only part of the cell-associated vectors were found to colocalize with caveolin-1, in agreement with data showing that only 1% to 10% of vector particles in a stock give rise to successful infection (57).

In summary, the data in Fig. 7 and 8 together with the okadaic acid data shown in Fig. 6A and 6B strongly suggest that the caveola-dependent entry of A-MLV in NIH 3T3 occurs through endocytosis.

DISCUSSION

Caveola-mediated entry of viruses was first demonstrated for SV40 (1, 41) and SV40 infection is presently the best-defined virus model for caveola-dependent entry and is used to define the properties of this entry pathway. We have here in a series of experiments shown that A-MLV infection of NIH 3T3, MDTF, and CHO K1 cells has the typical characteristics of a caveola-mediated infection as defined by studies on SV40 entry. We found that A-MLV infection is a slow process, pH independent, cholesterol dependent, and phosphatase sensi-

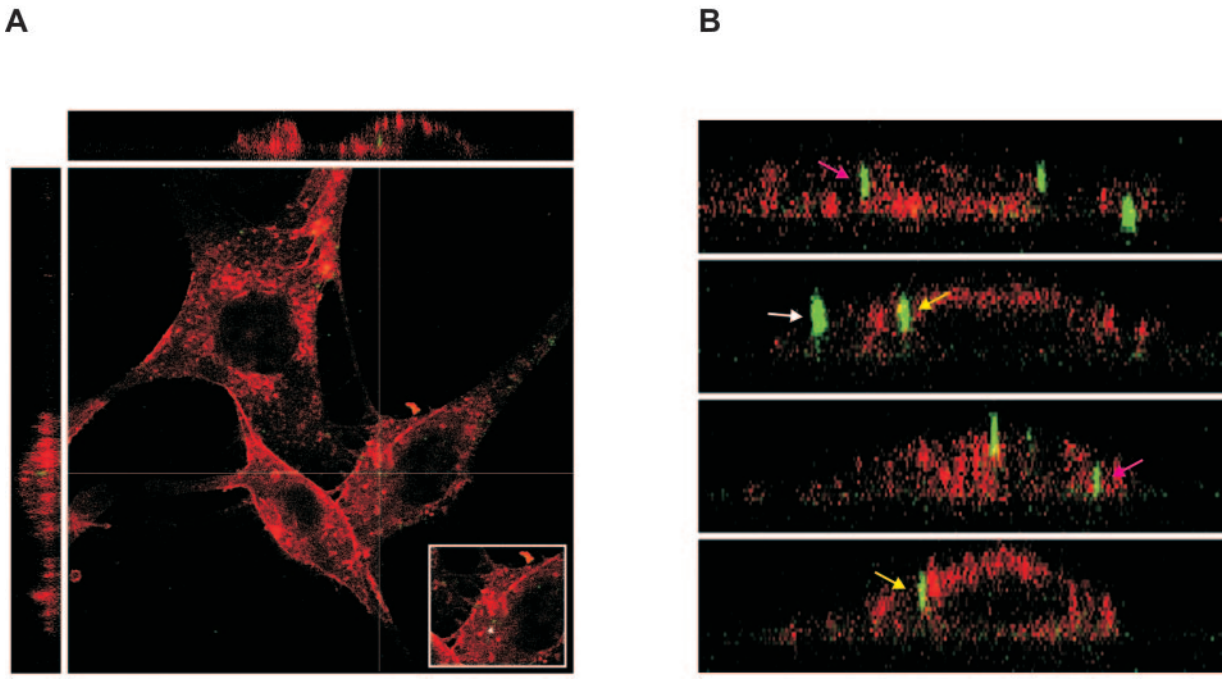

FIG. 7. Fusion-defective Gag-YFP A-MLV particles can enter NIH 3T3 mouse fibroblasts. (A and B) NIH 3T3 cells were incubated for 6 h with Gag-YFP A-MLV particles (green), which are fusion defective due to an unprocessed envelope protein. The cells were washed with citrate buffer and fixed with paraformaldehyde, and the plasma membrane was stained using rhodamine-labeled concanavalin A (red). The cells were investigated for the presence of intracellular fluorescent viral particles via three-dimensional scanning confocal microscopy. Shown are the YZ (left) and XZ (top) sections with the corresponding XY section. The insert in A shows the virus particle (arrow) at the XY cross-section. (B) XZ and YZ sections. Pink arrows: intracellular particles; yellow arrows: membrane-associated particles; white arrow: extracellular cell-bound particle.

tive in NIH 3T3 cells, moreover, it was inhibited by dominant-negative caveolin-1 in NIH 3T3 and CHO K1 cells. Furthermore, our okadaic acid experiments strongly implicate endocytic entry of A-MLV in NIH 3T3 cells.

Okadaic acid is a known inhibitor of phosphatases 1 and 2A (4) and okadaic acid treatment of cells removes caveolae from the cell surface and thereby transiently increases endocytosis of caveolae, while only an inhibitory effect on the clathrin-coated pits pathway has been described (38). Treatment of NIH 3T3 cells with okadaic acid prior to virus exposure decreased VSV as well as A-MLV infection, in agreement with VSV′s known entry pathway via clathrin-coated pits, and confirming the existence of an endocytic entry pathway for A-MLV. Moreover, treatment with okadaic acid after virus exposure increased A-MLV entry, as expected for a caveola-dependent endocytic pathway in that okadaic acid increases endocytosis of caveolae, whereas there was no effect on VSV infection. The latter is in agreement with our data on VSV infection kinetics in that at 4 h post-initiation of virus exposure the maximal infection level had been reached (Fig. 1) and thus no impairment of infection due to okadaic acid inhibition of endocytosis of clathrin-coated pits is expected.

In summary, the results from the okadaic acid experiments strongly suggest that A-MLV is able to enter cells via an endocytic pathway. Moreover, they are in agreement with a caveola-mediated entry pathway. These observations were further supported by the ability of fusion-defective A-MLV to enter NIH 3T3 cells and the observed colocalization of GFP-labeled fusion-defective A-MLV particles with caveolin-1. This is the first time a caveola-dependent entry pathway has been described for A-MLV. Moreover, we also show for the first time the association of the A-MLV receptor Pit2 with cholesterol-rich microdomains as well as its physical association with caveolin-1, the major protein of caveolae. Thus, the cellular

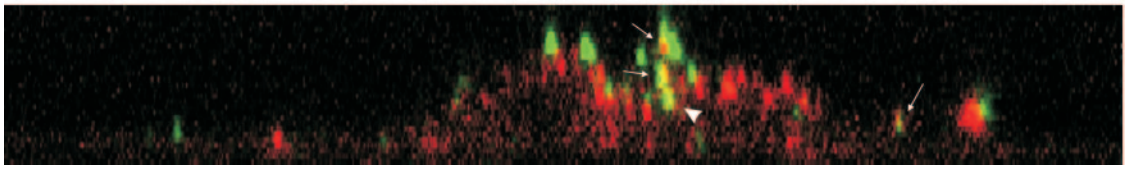

FIG. 8. Colocalization of fusion-defective Gag-YFP A-MLV particles with caveolin-1 in NIH 3T3 cells. NIH 3T3 cells were incubated for 6 h with Gag-YFP A-MLV particles (green), which are fusion defective due to an unprocessed envelope protein. The cells were permeabilized, fixed with paraformaldehyde, and stained for caveolin-1 (red). The cells were investigated using three-dimensional scanning confocal microscopy. Shown is one example of a YZ section showing colocalization of Gag-YFP A-MLV with caveolin-1. Arrows: Gag-YFP A-MLV particles colocalized with caveolin-1. Arrowhead: intracellular Gag-YFP A-MLV particle colocalized with caveolin-1.

behavior of the A-MLV receptor Pit2 supports its role in sustaining caveola-mediated viral entry.

We found that Pit2 protein was associated with cholesterol-rich membrane regions, but to what degree Pit2 is localized in other plasma membrane regions cannot be directly deduced from these data as the insoluble and soluble fractions also contain intracellular Pit2. In addition, Pit2 was found to be directly associated with caveolin-1. Proteins that are physically associated with caveolin-1 often possess a caveolin-binding motif (7); reviewed in reference (22). The caveolin-binding consensus sequences are ΦxΦxxxxΦ and ΦxxxxΦxxΦ, where Φ is an aromatic and x is any amino acid (7). Indeed, a consensus caveolin-binding motif is conserved in murine and human Pit2 (FaFfvwlF; amino acid positions 226 to 233 in both proteins), but no palmitoylation or myristoylation of Pit2, which could also direct it to cholesterol-rich microdomains, has been reported. Thus, the caveolin-binding motif is the only identified region in Pit2 with known caveola-targeting properties and we suggest that the direct association of Pit2 with caveolin-1 is most likely mediated by the identified caveolin-binding motif. We are currently investigating what role the plasma membrane localization of Pit2 plays in its function and regulation as a phosphate transporter.

The present results showing a caveola-mediated endocytic entry via Pit2 in CHO K1 cells is strengthened by the fact that disturbance of the actin cytoskeleton impaired A-MLV infection of CHO K1 cells (45) as caveolae are known to be anchored to the actin cytoskeleton and disruption of actin assembly blocks caveola-mediated endocytosis (54).

In an earlier report from McClure et al. it was suggested that A-MLV enters NIH 3T3 cells via direct fusion with the plasma membrane (25). This conclusion was based on the observation that A-MLV infection was not affected by NH_4Cl. On the other hand, the authors found infection of cells with E-MLV to be influenced by NH_4Cl treatment (25). Therefore, E-MLV has been described as a pH-dependent virus and A-MLV as a pH-independent virus. Katen and coworkers reexamined E-MLV and A-MLV entry in NIH 3T3 cells (16) and they reported that these viruses infect the host cells via the same infection route. Thus, they found that NH_4Cl treatment equally affected both MLV species but that this effect could be attributed mainly to a spontaneous inactivation of the viruses due to the experimental set-up. Therefore, they suggested a receptor-mediated endocytic pathway for E-MLV and A-MLV entry into NIH 3T3 cells and that the pathway does not necessarily involve acidic compartments such as endosomes and lysosomes. Indeed, for E-MLV it has been shown that the E-MLV receptor mCAT1 is directly associated with caveolin-1 and, in addition, infection with E-MLV was dependent on plasma membrane cholesterol (23). Thus, in light of the data presented here, we suggest that the previous results on E-MLV entry reflect a caveola-mediated entry pathway for E-MLV in NIH 3T3 cells.

Jobaggy and coworkers found that GFP-tagged Pit2 was present in an intracellular compartment after A-MLV infection of NIH 3T3 cells; the compartment was shown to be distinct from Golgi, endoplasmic reticulum, endosomes, and lysosomes (15). This observation is in agreement with a caveola-dependent A-MLV entry pathway in that caveola-mediated endocytosis can bypass the acidic compartments of cells (20, 34, 35, 40). For example, glycosyl-phosphatidyl-inositol-GFP and CD59 are transported from the plasma membrane to the Golgi in a clathrin-independent manner (35). These proteins accumulate in caveosomes (20, 34), which lack the classical markers for early and recycling endosomes but are positive for caveolin-1 (34). Indeed, very recent data point at caveolae as an elaborate system for sorting proteins from the plasma membrane while being able to maintain their integrity as caveolin-stabilized microdomains (40); the regulation of where caveolar vesicles end up in the cells, however, seems complex and is not fully elucidated. However, forcing SV40-containing caveolar vesicles to the endosomal compartment did not lead to SV40 infection, and thus SV40 exploits the fact that caveosomes can directly target the smooth endoplasmic reticulum (40). It is thought that the ability of caveosomes to bypass acidic compartments supports the intracellular survival of viruses and bacteria taking this entry route (40, 41, 46). Whether A-MLV targets caveosomes or other intracellular compartments after its endocytosis and how A-MLV escapes from endocytosed caveolar vesicles is presently not known.

We found that fusion-defective A-MLV is able to enter NIH 3T3 cells. The observed high ratio of plasma membrane-bound intracellular particles could imply that caveolar entry of A-MLV represents an unspecific accidental endocytosis of the particles. However, the observation that only a few particles were intracellular whereas the main part were bound to the plasma membrane is in agreement with the viruses entering via caveola-mediated endocytosis, in that the process has been shown to be infrequent and possibly regulated in fibroblastic cells (38). Moreover, nonspecific uptake of latex beads by caveolae has been shown to be strongly dependent on the particle size and no uptake of beads via caveolae is seen with beads having a diameter of 200 nm or smaller (44). Thus, the uptake of the fusion-defective fluorescent viral particles is not in agreement with an unspecific uptake of A-MLV via caveolae.

The majority of the viruses attached to the plasma membrane are probably bound to fibronectin produced by the NIH 3T3 fibroblasts, as it has been shown that MLV binds via heparin sulfate to fibronectin of the extracellular matrix (21). Indeed, Pizatto and coworkers have shown that virus-like particles without envelope protein can bind to cells (43).

From our data and the existing understanding of MLV infection, we suggest that A-MLV binds first to fibronectin and afterwards to Pit2. Moreover, we believe that this Pit2 protein is not initially associated with deep invaginated caveolae as these, with their average diameter of approximately 50 to 70 nm, are too small for a direct uptake of the 110-nm-diameter virus particles. It is, however, known that the size of caveolae can be increased after induction, as it has been shown for the uptake of *Streptococcus pyogenes* (46). Furthermore, for the caveola-mediated entry of SV40 it has been demonstrated that the majority of the viruses bind the receptors outside caveolae and are subsequently transported to caveolae where they are endocytosed (41). It is possible that similar mechanisms are involved in A-MLV entry and we are currently performing studies addressing the initial steps in Pit2-mediated entry.

In another study, deletion of about the middle half of human Pit2 was found to reduce A-MLV and 10A1 entry by 75% to 90% in CHO K1 cells compared to entry via wild-type human

Pit2 (5). In this Pit2 mutant, the caveolin-binding consensus sequence in positions 226 to 233 is deleted. We are currently investigating whether the remaining infection may represent an alternative entry route in CHO K1 cells or whether the mutant receptor reaches caveolae through another mechanism. Thus, while our data show that amphotropic MLVs enter at least NIH 3T3 and CHO K1 cells efficiently in a caveola-dependent manner, we do, however, believe that there also exist other entry pathways for these viruses. One reason for this is the ability of A-MLV and 10A1 MLV to infect hematopoietic cell lines, including T-lymphocytic lines (14, 58). Human and murine T lymphocytes, with the exception of activated T-cell leukemia lines, as well as many other established human hematopoietic cell lines seem not to express caveolin-1 at either the protein or the mRNA level (10, 12, 50). Thus, other entry mechanisms must exist which allow A-MLV infection in these cells. One possible alternative route could be entry via rafts in caveolin-negative cells. That retroviruses are able to use this entry route has been shown for avian sarcoma and leukemia virus (33).

ACKNOWLEDGMENTS

We thank Ari Helenius for GFP-cav-1 and cav-1-GFP, Mary Collins for Gag-YFP, Bryan O'Hara for pOJ74, Maribeth V. Eiden for the PA317GBN cell line, Melvyn Yap for MDTF cells, and David Kabat and Robert B. Gunn for Pit2-specific antibodies.

This work was supported by the Lundbeck Foundation, the Novo Nordisk Foundation, and the Danish Medical Research Council (grant 22-03-0254). C.B. was supported by German Academy of Natural Scientists grant BMBF-LPD 9901/8-81 using funds from the Bundesministerium für Bildung und Forschung.

REFERENCES

1. **Anderson, H. A., Y. Chen, and L. C. Norkin.** 1996. Bound simian virus 40 translocates to caveolin-enriched membrane domains, and its entry is inhibited by drugs that selectively disrupt caveolae. Mol. Biol. Cell **7:**1825–1834.
2. **Anderson, R. G. W.** 1998. The caveolae membrane system. Annu. Rev. Biochem. **67:**199–225.
3. **Andrawiss, M., Y. Takeuchi, L. Hewlett, and M. Collins.** 2003. Murine leukemia virus particle assembly quantitated by fluorescence microscopy: role of Gag-Gag interactions and membrane association. J. Virol. **77:**11651–11660.
4. **Bialojan, C., and A. Takai.** 1988. Inhibitory effect of a marine-sponge toxin, okadaic acid, on protein phosphatases. Specificity and kinetics. Biochem. J. **256:**283–290.
5. **Bøttger, P., and L. Pedersen.** 2004. The central half of Pit2 is not required for its function as a retroviral receptor. J. Virol. **78:**9564–9567.
6. **Bøttger, P., and L. Pedersen.** 2002. Two highly conserved glutamate residues critical for type III sodium-dependent phosphate transport revealed by uncoupling transport function from retroviral receptor function. J. Biol. Chem. **277:**42741–42747.
7. **Couet, J., S. Li, T. Okamoto, T. Ikezu, and M. P. Lisanti.** 1997. Identification of peptide and protein ligands for the caveolin-scaffolding domain. Implications for the interaction of caveolin with caveolae-associated proteins. J. Biol. Chem. **272:**6525–6533.
8. **Dickson, R. B., M. C. Willingham, and I. Pastan.** 1981. Alpha 2-macroglobulin adsorbed to colloidal gold: a new probe in the study of receptor-mediated endocytosis. J. Cell Biol. **89:**29–34.
9. **Eash, S., W. Querbes, and W. J. Atwood.** 2004. Infection of Vero cells by BK virus is dependent on caveolae. J. Virol. **78:**11583–11590.
10. **Fra, A. M., E. Williamson, K. Simons, and R. G. Parton.** 1994. Detergent-insoluble glycolipid microdomains in lymphocytes in the absence of caveolae. J. Biol. Chem. **269:**30745–30748.
11. **Gu, J. Z., E. D. Carstea, C. Cummings, J. A. Morris, S. K. Loftus, D. Zhang, K. G. Coleman, A. M. Cooney, M. E. Comly, L. Fandino, C. Roff, D. A. Tagle, W. J. Pavan, P. G. Pentchev, and M. A. Rosenfeld.** 1997. Substantial narrowing of the Niemann-Pick C candidate interval by yeast artificial chromosome complementation. Proc. Natl. Acad. Sci. USA **94:**7378–7383.
12. **Hatanaka, M., T. Maeda, T. Ikemoto, H. Mori, T. Seya, and A. Shimizu.** 1998. Expression of caveolin-1 in human T cell leukemia cell lines. Biochem. Biophys. Res. Commun. **253:**382–387.
13. **Ilangumaran, S., and D. C. Hoessli.** 1998. Effects of cholesterol depletion by cyclodextrin on the sphingolipid microdomains of the plasma membrane. Biochem. J. **335:**433–440.
14. **Introna, M., A. M. Barbui, J. Golay, F. Bambacioni, R. Schiro, S. Bernasconi, F. Breviario, E. Erba, G. Borleri, T. Barbui, A. Biondi, and A. Rambaldi.** 1998. Rapid retroviral infection of human haemopoietic cells of different lineages: efficient transfer in fresh T cells. Br. J. Haematol. **103:**449–461.
15. **Jobbagy, Z., S. Garfield, L. Baptiste, M. V. Eiden, and W. B. Anderson.** 2000. Subcellular redistribution of Pit-2 P_i transporter/amphotropic leukemia virus (A-MuLV) receptor in A-MuLV-infected NIH 3T3 fibroblasts: involvement in superinfection interference. J. Virol. **74:**2847–2854.
16. **Katen, L. J., M. M. Januszeski, W. F. Anderson, K. J. Hasenkrug, and L. H. Evans.** 2001. Infectious entry by amphotropic as well as ecotropic murine leukemia viruses occurs through an endocytic pathway. J. Virol. **75:**5018–5026.
17. **Kavanaugh, M. P., D. G. Miller, W. Zhang, W. Law, S. L. Kozak, D. Kabat, and A. D. Miller.** 1994. Cell-surface receptors for gibbon ape leukemia virus and amphotropic murine retrovirus are inducible sodium-dependent phosphate symporters. Proc. Natl. Acad. Sci. USA **91:**7071–7075.
18. **Keller, P., and K. Simons.** 1998. Cholesterol is required for surface transport of influenza virus hemagglutinin. J. Cell Biol. **140:**1357–1367.
19. **Kizhatil, K., and L. M. Albritton.** 1997. Requirements for different components of the host cell cytoskeleton distinguish ecotropic murine leukemia virus entry via endocytosis from entry via surface fusion. J. Virol. **71:**7145–7156.
20. **Le, P. U., and I. R. Nabi.** 2003. Distinct caveola-mediated endocytic pathways target the Golgi apparatus and the endoplasmic reticulum. J. Cell Sci. **116:**1059–1071.
21. **Lei, P., B. Bajaj, and S. T. Andreadis.** 2002. Retrovirus-associated heparan sulfate mediates immobilization and gene transfer on recombinant fibronectin. J. Virol. **76:**8722–8728.
22. **Liu, P., M. Rudick, and R. G. Anderson.** 2002. Multiple functions of caveolin-1. J. Biol. Chem. **277:**41295–41298.
23. **Lu, X., and J. Silver.** 2000. Ecotropic murine leukemia virus receptor is physically associated with caveolin and membrane rafts. Virology **276:**251–258.
24. **Marjomaki, V., V. Pietiainen, H. Matilainen, P. Upla, J. Ivaska, L. Nissinen, H. Reunanen, P. Huttunen, T. Hyypia, and J. Heino.** 2002. Internalization of echovirus 1 in caveolae. J. Virol. **76:**1856–1865.
25. **McClure, M. O., M. A. Sommerfelt, M. Marsh, and R. A. Weiss.** 1990. The pH independence of mammalian retrovirus infection. J. Gen. Virol. **71:**767–773.
26. **McLachlin, J. R., N. Mittereder, M. B. Daucher, M. Kadan, and M. A. Eglitis.** 1993. Factors affecting retroviral vector function and structural integrity. Virology **195:**1–5.
27. **Mellman, R., R. Fuchs, and A. Helenius.** 1986. Acidification of the endocytoic and exocytic pathways. Annu. Rev. Biochem. **55:**663–700.
28. **Miller, A. D., and C. Buttimore.** 1986. Redesign of retrovirus packaging cell lines to avoid recombination leading to helper virus production. Mol. Cell. Biol. **6:**2895–2902.
29. **Miller, A. D., and F. Chen.** 1996. Retrovirus packaging cells based on 10A1 murine leukemia virus for production of vectors that use multiple receptors for cell entry. J. Virol. **70:**5564–5571.
30. **Miller, A. D., and G. J. Rosman.** 1989. Improved retroviral vectors for gene transfer and expression. BioTechniques **7:**980–990.
31. **Miller, D. G., R. H. Edwards, and A. D. Miller.** 1994. Cloning of the cellular receptor for amphotropic murine retroviruses reveals homology to that for gibbon ape leukemia virus. Proc. Natl. Acad. Sci. USA **91:**78–82.
32. **Miller, D. G., and A. D. Miller.** 1994. A family of retroviruses that utilize related phosphate transporters for cell entry. J. Virol. **68:**8270–8276.
33. **Narayan, S., R. J. Barnard, and J. A. Young.** 2003. Two retroviral entry pathways distinguished by lipid raft association of the viral receptor and differences in viral infectivity. J. Virol. **77:**1977–1983.
34. **Nichols, B. J.** 2002. A distinct class of endosome mediates clathrin-independent endocytosis to the Golgi complex. Nat. Cell Biol. **4:**374–378.
35. **Nichols, B. J., A. K. Kenworthy, R. S. Polishchuk, R. Lodge, T. H. Roberts, K. Hirschberg, R. D. Phair, and J. Lippincott-Schwartz.** 2001. Rapid cycling of lipid raft markers between the cell surface and Golgi complex. J. Cell Biol. **153:**529–541.
36. **Nomura, R., A. Kiyota, E. Suzaki, K. Kataoka, Y. Ohe, K. Miyamoto, T. Senda, and T. Fujimoto.** 2004. Human coronavirus 229E binds to CD13 in rafts and enters the cell through caveolae. J. Virol. **78:**8701–8708.
37. **Olah, Z., C. Lehel, W. B. Anderson, M. V. Eiden, and C. A. Wilson.** 1994. The cellular receptor for gibbon ape leukemia virus is a novel high affinity sodium-dependent phosphate transporter. J. Biol. Chem. **269:**25426–25431.
38. **Parton, R. G., B. Joggerst, and K. Simons.** 1994. Regulated internalization of caveolae. J. Cell Biol. **127:**1199–1215.
39. **Pedersen, L., S. V. Johann, M. van Zeijl, F. S. Pedersen, and B. O'Hara.** 1995. Chimeras of receptors for gibbon ape leukemia virus/feline leukemia virus B and amphotropic murine leukemia virus reveal different modes of receptor recognition by retrovirus. J. Virol. **69:**2401–2405.
40. **Pelkmans, L., T. Burli, M. Zerial, and A. Helenius.** 2004. Caveolin-stabilized

membrane domains as multifunctional transport and sorting devices in endocytic membrane traffic. Cell **118:**767–780.
41. **Pelkmans, L., J. Kartenbeck, and A. Helenius.** 2001. Caveolar endocytosis of simian virus 40 reveals a new two-step vesicular-transport pathway to the ER. Nat. Cell Biol. **3:**473–483.
42. **Pelkmans, L., D. Puntener, and A. Helenius.** 2002. Local actin polymerization and dynamin recruitment in SV40-induced internalization of caveolae. Science **296:**535–539.
43. **Pizzato, M., S. A. Marlow, E. D. Blair, and Y. Takeuchi.** 1999. Initial binding of murine leukemia virus particles to cells does not require specific Env-receptor interaction. J. Virol. **73:**8599–8611.
44. **Rejman, J., V. Oberle, I. S. Zuhorn, and D. Hoekstra.** 2004. Size-dependent internalization of particles via the pathways of clathrin- and caveola-mediated endocytosis. Biochem. J. **377:**159–169.
45. **Rodrigues, P., and J. M. Heard.** 1999. Modulation of phosphate uptake and amphotropic murine leukemia virus entry by posttranslational modifications of PIT-2. J. Virol. **73:**3789–3799.
46. **Rohde, M., E. Mueller, G. S. Chhatwal, and S. R. Talay.** 2003. Host cell caveolae act as an entry-port for group A streptococci. Cell Microbiol. **5:**323–342.
47. **Rothberg, K. G., J. E. Heuser, W. C. Donzell, Y. S. Ying, J. R. Glenney, and R. G. Anderson.** 1992. Caveolin, a protein component of caveolae membrane coats. Cell **68:**673–682.
48. **Sandrin, V., S. J. Russell, and F. L. Cosset.** 2003. Targeting retroviral and lentiviral vectors. Curr. Top. Microbiol. Immunol. **281:**137–178.
49. **Sandvig, K., S. Olsnes, O. W. Petersen, and B. van Deurs.** 1987. Acidification of the cytosol inhibits endocytosis from coated pits. J. Cell Biol. **105:**679–689.
50. **Simmons, G., A. J. Rennekamp, N. Chai, L. H. Vandenberghe, J. L. Riley, and P. Bates.** 2003. Folate receptor alpha and caveolae are not required for Ebola virus glycoprotein-mediated viral infection. J. Virol. **77:**13433–13438.
51. **Simons, K., and E. Ikonen.** 1997. Functional rafts in cell membranes. Nature **387:**569–572.
52. **Smart, E. J., G. A. Graf, M. A. McNiven, W. C. Sessa, J. A. Engelman, P. E. Scherer, T. Okamoto, and M. P. Lisanti.** 1999. Caveolins, liquid-ordered domains, and signal transduction. Mol. Cell. Biol. **19:**7289–7304.
53. **Soneoka, Y., P. M. Cannon, E. E. Ramsdale, J. C. Griffiths, G. Romano, S. M. Kingsman, and A. J. Kingsman.** 1995. A transient three-plasmid expression system for the production of high titer retroviral vectors. Nucleic Acids Res. **23:**628–633.
54. **Stahlhut, M., and B. van Deurs.** 2000. Identification of filamin as a novel ligand for caveolin-1: evidence for the organization of caveolin-1-associated membrane domains by the actin cytoskeleton. Mol. Biol. Cell **11:**325–337.
55. **Thomsen, P., K. Roepstorff, M. Stahlhut, and B. van Deurs.** 2002. Caveolae are highly immobile plasma membrane microdomains, which are not involved in constitutive endocytic trafficking. Mol. Biol. Cell **13:**238–250.
56. **Timmer, R. T., and R. B. Gunn.** 2000. The molecular basis for Na-dependent phosphate transport in human erythrocytes and K562 cells. J. Gen. Physiol. **116:**363–378.
57. **Towers, G. J., D. Stockholm, V. Labrousse-Najburg, F. Carlier, O. Danos, and J.-C. Pagès.** 1999. One step screening of retroviral prodicer clones by real time quantitative PCR. J. Gene Med. **1:**352–359.
58. **Uckert, W., C. Becker, M. Gladow, D. Klein, T. Kammertoens, L. Pedersen, and T. Blankenstein.** 2000. Efficient gene transfer into primary human CD8+ T lymphocytes by MuLV-10A1 retrovirus pseudotype. Hum. Gene Ther. **11:**1005–1014.
59. **van Zeijl, M., S. V. Johann, E. Closs, J. Cunningham, R. Eddy, T. B. Shows, and B. O'Hara.** 1994. A human amphotropic retrovirus receptor is a second member of the gibbon ape leukemia virus receptor family. Proc. Natl. Acad. Sci. USA **91:**1168–1172.
60. **Wilson, C. A., M. V. Eiden, W. B. Anderson, C. Lehel, and Z. Olah.** 1995. The dual-function hamster receptor for amphotropic murine leukemia virus (MuLV), 10A1 MuLV, and gibbon ape leukemia virus is a phosphate symporter. J. Virol. **69:**534–537.